

# Chapter 1

## Nanophotonics and Single Molecules

W.E. Moerner(✉), P. James Schuck, David P. Fromm,  
Anika Kinkhabwala, Samuel J. Lord, Stefanie Y. Nishimura,  
Katherine A. Willets, Arvind Sundaramurthy, Gordon Kino,  
Meng He, Zhikuan Lu, and Robert J. Twieg

### Contents

1.1	Introduction.....	2
1.2	Development of Single-Molecule Fluorophores with Alternate Readout Capabilities .....	3
1.2.1	Motivations .....	3
1.2.2	The DCDHF Single-Molecule Fluorophores.....	3
1.2.3	Comparing DCDHF Molecules to Well-Known Single-Molecule Fluorophores .....	5
1.2.4	Lifetimes in Different Environments .....	6
1.2.5	Labeling of Cellular Membranes .....	7
1.2.6	Two-Photon Fluorescence Excitation .....	10
1.3	Toward Improving the Mismatch Between Light and Single Molecules .....	11
1.3.1	Motivation.....	11
1.3.2	Optically Resonant Metallic Bowtie Nanoantennas .....	13
1.3.3	Optical Resonances of Metallic Bowtie Nanoantennas.....	13
1.3.4	Local Enhancement of the Optical Fields Near the Nanoantenna .....	14
1.3.5	Exploring the Chemical Enhancement for Surface-Enhanced Raman Scattering with Au Bowtie Nanoantennas .....	16
1.4	Summary and Prospects.....	19
1.4.1	Single-Molecule Fluorophores .....	19
1.4.2	Metallic Bowtie Nanoantennas .....	19
	References.....	20

**Abstract** Single emitting molecules are currently providing a new window into nanoscale systems ranging from biology to materials science. The amount of information that can be extracted from each single molecule depends upon the specific photophysical properties of the fluorophore and how these properties are affected by the nearby environment. For this reason, it is necessary to develop single-molecule emitters with as many different reporter functions as possible. The first part of this chapter describes a relatively new class of single-molecule fluorophores which offer

---

W.E. Moerner  
Department of Chemistry, Stanford University, Stanford, CA, 94305-5080 USA  
wmoerner@stanford.edu

R. Rigler and H. Vogel (eds.), *Single Molecules and Nanotechnology*. 1  
*Springer Series in Biophysics 12*.  
© Springer-Verlag Berlin Heidelberg 2008

tunable photophysical properties and, in turn, improved local reporting functionality on the nanometer length scale. The second part of this chapter presents metallic nanostructures which can address a second issue: the mismatch between the typical size of a single fluorophore ( $\sim 1$  nm along a long dimension) and the wavelength of light ( $\sim 500$  nm). Such nanostructures could lead to more efficient excitation of single molecules, in particular, higher excitation probability as well as reduced backgrounds, and effectively higher spatial resolution. Metallic nanostructures based on two triangles formed into a bowtie shape feature large enhancements of the local electromagnetic field and give rise to strong surface-enhanced Raman scattering of molecules. In future work, enhanced electromagnetic structures can be combined with single-molecule reporters in a variety of applications.

## 1.1 Introduction

In recent decades, the ability to perform optical spectroscopy and microscopy of single molecules in condensed phase samples (Moerner and Orrit 1999) has fascinated scientists in fields ranging from biophysics (Zhuang and Rief 2000; Weiss 1999; Lu 2005; Rasnik et al. 2005), to cellular biology (Moerner 2003), to materials and polymer science (Cotlet et al. 2004; Barbara et al. 2005; Lee et al. 2005), and even to quantum-mechanical single-photon sources (Moerner 2004; Lounis and Orrit 2005). Using now-standard experimental methods (Ha et al. 1999; Ha 2001; Moerner and Fromm 2003), information on local interactions can be extracted, molecule by molecule, by the measurement of excited state lifetimes, spectra, orientations, brightness, degree of energy transfer, and photon correlations, thus removing ensemble averaging and allowing exploration of heterogeneity. Single-molecule studies often reveal complex statistical fluctuations, which allow useful comparison with theoretical models in a variety of cases (Barkai et al. 2004; Watkins and Yang 2004; Hummer and Szabo 2005).

A continuing need exists for the improvement and extension of these efforts in order to increase the variety and amount of information that may be obtained from single-molecule studies. For example, at room temperature, eventual photobleaching limits the knowledge that may be extracted from each individual molecule. To compensate for this, it is necessary to continually develop new reporter functions for robust fluorophores that provide sufficiently strong signals at the single-molecule level.

The first part of this chapter describes a relatively new class of single-molecule fluorophores which offer tunable photophysical properties and, in turn, improved local reporting functionality on the nanometer length scale. While a single molecule can report on its immediate nanoenvironment, in most experiments, there is a large mismatch between the size of a single fluorophore ( $\sim 1$  nm along a long dimension) and the wavelength of light ( $\sim 500$  nm). Developing ways to overcome this would lead to more efficient excitation of single molecules, in particular, higher excitation probability as well as reduced backgrounds, and effectively higher spatial resolution.

One approach for overcoming the mismatch involves nanoscale metallic structures that concentrate light to subwavelength regions. We have explored this idea with metallic “bowtie” nanoantennas in which the enhancement of the local electromagnetic field can be directly measured. In the second part of this chapter we describe the optical properties of bowties, and illustrate their use in spectroscopy for the case of surface-enhanced Raman scattering of molecules. In future work, enhanced electromagnetic structures can be combined with single-molecule reporters in a variety of applications.

## **1.2 Development of Single-Molecule Fluorophores with Alternate Readout Capabilities**

### ***1.2.1 Motivations***

Over the years, it is certainly true that a large number of fluorescent dyes (Tsien and Waggoner 1995) have become available for labeling applications, for example, from commercial sources such as Molecular Probes (Invitrogen Corp.), Dyomics GmbH, and many others. Of particular interest here are the fluorophores that show environmental sensitivity, that is, those which show alterations in emission spectra, fluorescence lifetimes, or fluorescence quantum yields that vary based on the polarity or the viscosity of the environment. For example, dyes such as laurdan, prodan, dansyl, NBD, merocyanines, and the recently reported di-4-ANEPPHQ have all been utilized in various reporter applications in biological systems (Parasassi et al. 1998; Maier et al. 2002; Touthkine et al. 2003; Jin et al. 2005), but this list is by no means exhaustive. For the most part, experiments using environmentally sensitive fluorophores have focused on high concentration imaging, as only a subset of the larger group of fluorophores shows the high quantum yield, weak triplet bottlenecks, and high photostability to allow detection at the single-molecule level. For this reason, it is necessary to continue research efforts to develop single-molecule emitters with as many different reporter functions as possible.

### ***1.2.2 The DCDHF Single-Molecule Fluorophores***

Recent work in the Moerner and Twieg laboratories has focused on a new class of fluorophores that meet the strict demands for single-molecule imaging and offer additional interesting properties such as a large ground state dipole moment  $\mu_g$ , moderate hyperpolarizability  $\beta$ , and sensitivity to the rigidity of the local environment (Willets et al. 2003a, 2005). The molecules within this class all contain an amine donor and a dicyanodihydrofuran (DCDHF) acceptor linked by a conjugated unit (benzene, thiophene, styrene, etc.). These molecules are named DCDHF fluorophores after the acceptor unit (Melikian et al. 1995), which is constant among the

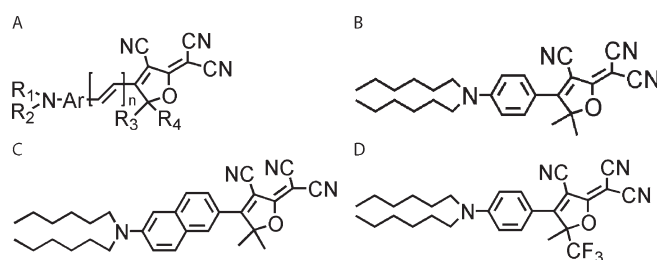


**Figure 1.1** Representative structures of the DCDHF fluorophore class. In the general structure **A**, the aromatic group (Ar) may be one or more benzene or thiophene groups, and different substituents may be added at the positions R1–R4 to modify the properties of the molecule. The structure **B** shows the first molecule studied in this class, DCDHF-6. Structure **C**, DCDHF-N-6, is a long-wavelength version; structure **D**, DCDHF-CF<sub>3</sub>, has been used in membrane labeling studies as described in the text

class. Figure 1.1A shows the general structure of these molecules, and Figure 1.1B shows the molecule DCDHF-6, the first and most studied compound in this group. The DCDHF molecules are examples of nonlinear optical chromophores possessing large second-order nonlinearity by virtue of the asymmetric donor–acceptor structure and high degree of conjugation (Nicoud and Twieg 1987; Kanis et al. 1994; Zyss 1994; Zhang et al. 2001).

Nonlinear optical chromophores at high concentrations in polymers have received much attention from the chemical community in recent decades owing to the utility of such materials for second-harmonic generation, electro-optic phase modulation, and many other potential applications (Prasad and Williams 1991; Burland et al. 1994; Nalwa and Miyata 1997; Kuzyk and Dirk 1998). The DCDHF molecules were originally designed for and utilized extensively in high-performance photorefractive polymer materials (Wright et al. 2001; He et al. 2002; Ostroverkhova et al. 2002; Ostroverkhova and Moerner 2004).

Usually, nonlinear optical chromophores are not thought to be particularly fluorescent, inasmuch as the strong charge-transfer transition producing the optical nonlinearity is often accompanied by considerable excited-state distortion of the molecule. In spite of this, the DCDHF fluorophores are surprisingly well-suited for single-molecule fluorescence detection (Willets et al. 2003). This may be a result of the fact that their earlier optimization for photorefractive applications rested more upon producing a large polarizability anisotropy and dipole moment rather than a large hyperpolarizability (Kippelen et al. 1997). Figure 1.2A shows an epifluorescence image of single molecules of DCDHF-6 in a poly(methyl methacrylate) thin film at room temperature. Observing the time-dependent emission from single spots (Figures 1.2B, 1.2C) shows clear single-step photobleaching. The blinking event for Figure 1.2C near 3 seconds is a property common to many single molecules (Moerner 1997), but in this system, 85% of the molecules observed did not show blinking on the time scale of the measurement (100 ms), itself a surprising result.

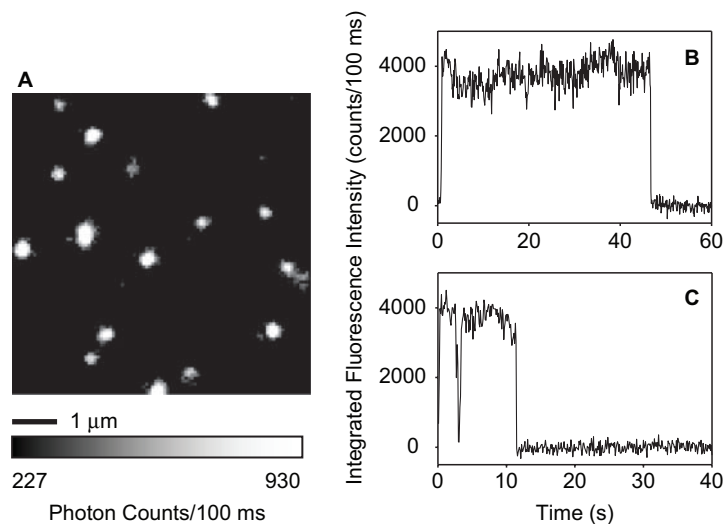


**Figure 1.2** (A) Epifluorescence image of single molecules of DCDHF-6 in a thin film of PMMA at room temperature. The time traces in (B) and (C) show single-step photobleaching. (Reprinted by permission from Willets et al. (2003a))

### 1.2.3 Comparing DCDHF Molecules to Well-Known Single-Molecule Fluorophores

To illustrate some of the properties of molecules in the DCDHF class compared to conventional fluorophores, Table 1.1 shows the properties of three DCDHFs compared to Rhodamine 6G (R6G) and Texas Red.

Although the absorption and emission of R6G and Texas Red are at longer wavelengths than for DCDHF-6, the synthetic flexibility of the DCDHFs at the conjugated linker (Ar plus  $n$  vinyl groups; Figure 1.1A) has allowed derivatives to be produced with absorption as long as 700 nm (for a thiophene–thiophene–vinyl linker) while maintaining the advantageous characteristics of the parent molecule. The fourth entry in the table for DCDHF-N-6 (see Figure 1.1C) is an example of one of the long-wavelength emitters where the aromatic coupling group is a naphthalene (Lord et al. 2007). The fifth entry is for DCDHF-A-6, the anthracene analogue to DCDHF-N-6. Comparing the first three rows in the table, the extinction coefficients  $\epsilon$  for R6G and Texas Red are larger than for DCDHF-6, but this parameter too is larger for other longer wavelength versions of the DCDHF molecules not shown here.

Surprisingly, in toluene liquid solution, the fluorescence quantum yield  $\Phi_F$  for DCDHF-6 is quite small. The first clue that these molecules have strong environmental sensitivity came from the observation that in the relatively more rigid PMMA environment, the fluorescence quantum yield is much higher, comparable to R6G and Texas Red. It is important to note that the bulk photobleaching quantum yields  $\Phi_B$  are

**Table 1.1** Properties of three DCDHFs compared to rhodamine 6G (R6G) and Texas Red

	$\lambda_{\text{abs}}(\text{nm})$	$\lambda_{\text{em}}(\text{nm})$	$\epsilon (\text{M}^{-1}\text{cm}^{-1})$	$\Phi_{\text{F}}$	$\Phi_{\text{B}}$	$N_{\text{tot,e}}$	$\mu_{\text{g}}(\text{D})$
R6G	530	556	105,000	0.95	$5 \times 10^{-7\text{a}}$ $1 \times 10^{-5\text{b}}$	$1.9 \times 10^6$	cation
Texas Red	576	592	177,000	0.93	$7 \times 10^{-7\text{a}}$ $4 \times 10^{-5\text{b}}$	$1.4 \times 10^6$	anion
DCDHF-6	486	505	71,000	0.044 <sup>c</sup> 0.92 <sup>d</sup>	$9 \times 10^{-7\text{d}}$	$2.4 \times 10^{6\text{d,e}}$	11.4
DCDHF-N-6	526	579	42,000	0.85 <sup>c</sup> 0.98 <sup>d</sup>	$2 \times 10^{-6\text{b}}$	$1.4 \times 10^{6\text{d,f}}$	–
DCDHF-A-6	585	689	35,000	0.54 <sup>c</sup> 0.71 <sup>d</sup>	$1 \times 10^{-5\text{b}}$	$2.2 \times 10^{6\text{d,g}}$	–

<sup>a</sup>In ethanol (Soper et al. 1993)<sup>b</sup>In aqueous gelatin<sup>c</sup>In toluene<sup>d</sup>In a PMMA film<sup>e</sup>Corrected for a detection efficiency of 8%<sup>f</sup>Corrected for a detection efficiency of 9%<sup>g</sup>Corrected for a detection efficiency of 10%

also quite comparable, and superior when compared in an aqueous environment. The inverse of this parameter is approximately related to the average number of emitted photons before photobleaching in the single-molecule experiments,  $N_{\text{tot,e}}$ . Again, the DCDHF-6 dye is quite comparable to the conventional fluorophores. Finally, although DCDHF-6 has a large ground state dipole moment, R6G and Texas Red are charged.

The mechanism for the increase in fluorescence emission in more rigid environments has been explored by quantum chemical calculations of the energy level structure of the molecule as a function of various intramolecular twists (Willets et al. 2004). By calculating the various excited state geometries that could be easily reached upon a Franck–Condon excitation, two relaxed forms were found, one with a more planar molecular structure, and one with a large twist around the dicyanomethylene bond. The former is likely to be emissive, whereas the latter is not far in energy from a similar structure on the ground state manifold, and hence would be expected to be nonradiative. The model was considered that the varying emission from the molecule results from changing the partitioning between the two de-excitation pathways. Presumably, in a more rigid environment that restricts the dicyanomethylene twist, the molecule cannot access the nonradiative pathway. The fact that the  $\Phi_{\text{F}}$  value for the DCDHF-6 molecule shows a strong correlation with the viscosity when in hydrogen-bonding solvents might be a result of local steric hindrance from the immediate H-bond network. These ideas are subjects of future theoretical and experimental verification.

### 1.2.4 Lifetimes in Different Environments

The reporter properties of the DCDHF fluorophores can be exploited in single-molecule experiments to reveal inherent differences in local environments or to

monitor time-dependent changes in the host. Because the fluorescence quantum yield is related to the excited state lifetime ( $\tau_F$ ) of a molecule ( $\Phi_F = \tau_F / \tau_{rad}$ , with  $\tau_{rad}$  the radiative lifetime; Lakowicz 1999), the  $\tau_F$  value should also provide a sensitive measure of the local environment. Using conventional time-correlated single photon counting (TCSPC) methods to record delay times between excitation by a pulsed laser source and emission from a single molecule (Lakowicz 1999), the excited state lifetimes of the DCDHF-6 molecules in different hosts can be measured. In toluene, where the measured quantum yield was quite low, the bulk excited state lifetime was limited by the response time of the instrument ( $<400$  ps); on the other hand, in PMMA where the quantum yield was near unity, the lifetime was several ns (Willets et al. 2003, 2004).

Bulk studies of DCDHF-6 in different methacrylate polymer hosts revealed that the average excited state lifetime of the molecule increased with increasing glass transition temperature ( $T_g$ ) of the host. However, ensemble studies do not directly yield insight into the overall heterogeneity of the environment, because only the average value of the lifetime is measured. For single-molecule experiments, dilute samples of DCDHF-6 were prepared in PMMA ( $T_g \sim 120^\circ\text{C}$ ) and an (*n*-butyl methacrylate)/(iso-butyl methacrylate) copolymer ( $T_g \sim 35^\circ\text{C}$ ), and both samples were studied at room temperature. Figure 1.3A shows an example of a lifetime measurement for a single molecule in PMMA, which fits a single exponential very well. Figure 1.3B shows the distribution of single-molecule lifetimes in the two different hosts as well as fits to a Gaussian profile.

Consistent with the bulk results, the average lifetime in the copolymer is shorter than in the PMMA. The widths of both distributions, however, are greater than the statistically expected measurement error of 100 ps, which can be attributed to the microscopic heterogeneity of the polymer films. The distribution of lifetimes is broader in the copolymer host, suggesting that a greater variety of microscopic local environments exists in this matrix.

Recent work has shown that the lifetime of a twisted perylene derivative reports on the free volume of its host polymer matrix (Vallee et al. 2004); this idea may also apply to the DCDHF results. The local free volume in the copolymer is expected to be higher than that in the PMMA (Vallee et al. 2004) and thus our results suggest that the free volume is not only larger but also more broadly distributed in the copolymer. This example shows that these dyes may prove useful for sensing dynamic changes in the local environment, simply by monitoring changes in the excited state lifetime of an individual molecule as its host environment is perturbed. Such measurements are useful not only for studying polymers, but for any situation in which dynamic changes in environment are expected.

### 1.2.5 Labeling of Cellular Membranes

Many types of dynamic environments exist in biological systems, where many dynamical processes and heterogeneous environments can be found. Although synthetic modifications to optimize interaction of the DCDHF dyes with specific

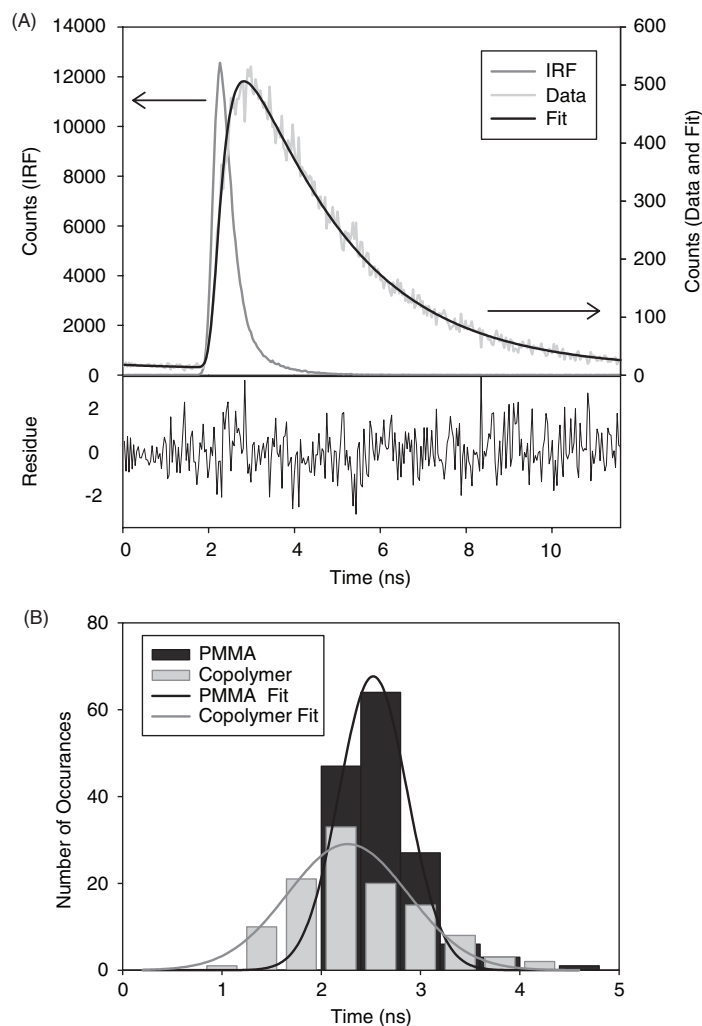


**Figure 1.3** (A) Excited state lifetime measurement (light gray line) of a single molecule of DCDHF-6 in PMMA. Also shown are the instrument response function (dark gray line) and a single exponential fit to the data (black line) with a characteristic decay time of 2.42 ns. The residuals of the fit are also shown. (Reprinted by permission from Willets et al. (2003b)). (B) Histogram of single molecule fluorescence lifetimes of DCDHF-6 in a BM/iBM copolymer (light gray) and in PMMA (dark gray). For both datasets, 400 ps bins are used. The error of the individual lifetime determinations is 100 ps. (Reprinted by permission from Willets et al. (2005))

biological targets are underway, the fluorophores in their current form are directly useful in the study of cellular membranes. The molecules have an amphiphilic structure with a polar dicyanomethylenedihydrofuran group at one end and a non-polar hydrocarbon tail on the amine. Thus, the DCDHF dyes can act as fluorescent

lipid analogues, and the relatively constrained environment of the membrane bilayer can lead to bright emission.

Using egg phosphatidylcholine vesicles to deliver the fluorophores to a cell membrane (Schütz et al. 2000) or by dissolution in a small amount of ethanol, single-molecule concentrations of DCDHF probes have been successfully inserted into the plasma membrane of Chinese hamster ovary (CHO) cells. To illustrate, part A of Figure 1.4 shows a white-light transmission image of a CHO cell (typical dimensions  $\sim 10 \times 25 \mu\text{m}$  in the image plane, and  $\sim 5 \mu\text{m}$  thick). Figure 1.4B shows a wide-field fluorescence image of single molecules of DCDHF6-CF3 in the upper plasma membrane of this CHO cell. Each molecule is rapidly diffusing in the membrane, and by recording positional trajectories as a function of time, the diffusion coefficient for the DCDHF molecules in the membrane can be calculated (Vrljic et al. 2002). The observed diffusion coefficient of  $2.1 \mu\text{m}^2\text{s}^{-1}$  is consistent with measured diffusion coefficients of other fluorescent lipid analogues such as Cy5-labeled DOPE (Schütz et al. 2000) in the plasma membrane, which suggests that the DCDHF molecules are integrated into the lipid bilayer.

The compatibility of the DCDHF dyes with cells as well as the synthetic flexibility to add reactive functional groups for site-specific labeling should allow the DCDHF fluorophores to be useful for a variety of in vitro and in vivo biological labeling experiments. In addition, future studies should also be able to detect changes in the

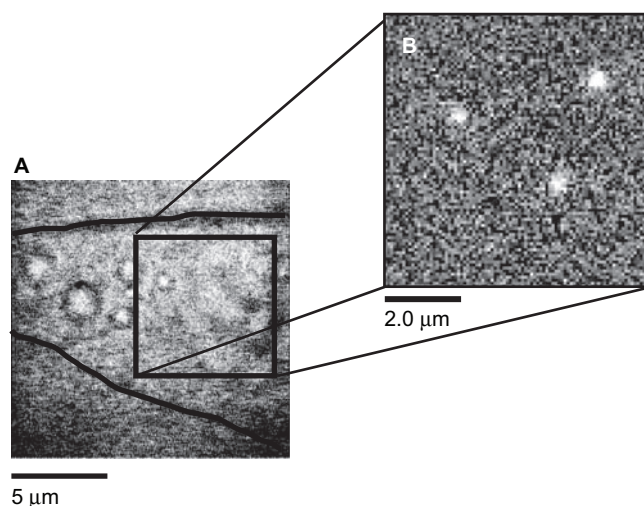


**Figure 1.4** (A) White-light transmission image of a CHO cell showing the sketched cell edges (black) and the region of interest. (B) Epifluorescence image of single molecules of DCDHF6-CF3 in the upper membrane of the cell excited at 532 nm with an 18 ms integration time. (Parts (A) (B) reprinted by permission from Willets et al. (2005))

emission properties arising from local heterogeneity in the plasma membrane (Nishimura et al. 2006).

### ***1.2.6 Two-Photon Fluorescence Excitation***

One of the challenges of labeling live cells with single-molecule reporters is the large autofluorescence background arising from natively fluorescent molecules such as flavins. Because these interfering fluorescent molecules are so plentiful, their emission can overwhelm the relatively small fluorescence signal from single-molecule labels. One solution to this problem involves preparation of long-wavelength emitters, and the DCDHF molecules do allow for this possibility.

Alternatively, many researchers have turned to two-photon fluorescence in order to avoid the naturally occurring background (Denk et al. 1990; Xu et al. 1996). In these experiments, two (typically infrared) photons of frequency  $\omega$  are used to excite the molecule rather than a single photon with the optically resonant frequency  $2\omega$ . Infrared excitation can reduce signals from the autofluorescent species in the cell, however, two-photon absorption is a low probability event, typically requiring high intensity excitation with  $\sim 100$  fs laser pulses, and therefore the single emitter of interest needs to have a large two-photon absorption cross-section  $\delta$ . For example, the  $\delta$  value for R6G in methanol, considered a fairly strong two-photon emitter, is 30 GM at 800 nm (where 1 GM =  $10^{-50}$  cm<sup>4</sup> s photon<sup>-1</sup>; Albota et al. 1998).

The natural optical nonlinearity of the DCDHF dyes suggests that they too may be useful two-photon emitters, and our recent measurements find two-photon cross-sections reaching more than 44 GM for DCDHF-6, slightly larger than that for R6G (Schuck et al. 2005b). Figure 1.5a shows the expected quadratic behavior of the bulk DCDHF-6 two-photon absorption signal versus input cw laser power from 930 nm pulses from a mode-locked Ti:Sapphire laser (pulse widths  $\sim 125$  fs). In Figure 1.5b, the fluorescence spectra arising from one- and two-photon excitation are shown to be roughly identical. The TPF excitation spectrum peaks at 945 nm and approximately mirrors the shape of the single-photon absorption spectrum with double the wavelength. As with many two-photon dyes (Xu and Webb 1996a; Schuck et al. 2005b), the spectrum is blue-shifted by more than 40 nm relative to the expectation from single-photon absorption. In Figure 1.5c, for a single-molecule concentration sample of DCDHF-6 in PMMA, the two-photon excited fluorescence from individual molecules is easily observed, with clear single-step photobleaching (Figure 1.5d). The ability to observe single molecules of DCDHF-6 using two-photon fluorescence expands the range of usefulness of these dyes, suggesting that they are candidates for applications where autofluorescence provides excessive background.

Overall, these studies and others in progress show that the DCDHF dyes are excellent single-molecule emitters with a degree of synthetic flexibility that should allow them to be tailored for a variety of applications.

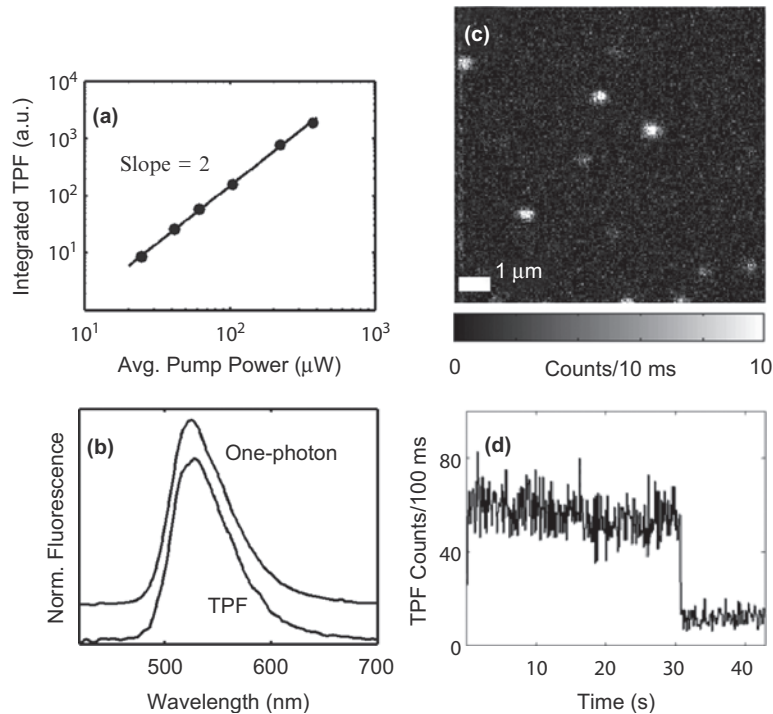


**Figure 1.5** (a) A log–log plot demonstrating the quadratic dependence of TPF on average excitation power for a bulk sample of DCDHF-6 in PMMA. (b) One- and two-photon fluorescence spectra from DCDHF-6, where the one-photon spectrum has been vertically offset for clarity. (c) TPF scanning confocal image of single DCDHF-6 molecules in a PMMA film. (d) Area-integrated TPF intensity of a single molecule as a function of time, 100 ms averaging interval. (Reprinted by permission from Schuck et al. (2005b))

### 1.3 Toward Improving the Mismatch Between Light and Single Molecules

#### 1.3.1 Motivation

When light of wavelength  $\lambda$  is focused into a medium of refractive index  $n$ , the minimum spot size due to diffraction is of the order of  $\lambda/(2n)$ . For example, at a wavelength of 405 nm, at the edge of the visible band, diffraction limits the minimum spot size to be greater than  $\sim 150$  nm. Typical single-molecule emitters are far smaller, and it would be far more efficient to couple the single molecule to a near-field light source far smaller than the diffraction-limited value. Aperture-based near-field techniques, where light is squeezed through a tiny hole, can achieve lateral spatial resolution on the order of the hole diameter (Betzig et al. 1991). In practice, near-field microscopic images have been recorded by pulled and metal-coated optical fiber tips, but these are fragile and plagued by poor transmission, on the order of  $10^{-3}$  to  $10^{-6}$  (Zenhausern et al. 1995).

Electromagnetic theory predicts that electric fields (E-fields) are enhanced in close proximity to sharp metal points with a radius of curvature much smaller than the incident illumination wavelength, the so-called lightning-rod effect that has been recently applied at optical frequencies, producing lateral resolution on the order of the curvature of the point (Bohn et al. 2001). The highly localized E-field enhancement in apertureless near-field systems has been exploited to produce an ultra-small, ultra-intense light source that has applications in high-density optical storage, high-resolution optical imaging, and laser spectroscopy, including enhanced fluorescence (Novotny et al. 1998) and Raman scattering (Hartschuh et al. 2003).

Small metallic particles with sharp points also produce locally enhanced E-fields, and rod-shaped and triangular antennas have recently been made resonant in the infrared (Crozier et al. 2003). In the microwave regime, it has been shown that a “bowtie”-shaped antenna, where two metallic triangles facing tip to tip are separated by a small gap, produces a large E-field confined to the area near the gap (Grober et al. 1997). Small gaps between two nanometer-scale particles have also been implicated in producing electromagnetically enhanced “hot spots,” enabling the detection of surface enhanced Raman scattering (SERS) of single molecules (Kneipp et al. 1997; Nie and Emory 1997; Michaels et al. 2000).

Investigators have suggested that the ultra-intense fields required for SERS are created by strong plasmonic coupling between pairs of small metallic spheres (Michaels et al. 2000; Kneipp et al. 2002; Xu and Kaelin 2003). However, all single-molecule SERS studies to date have used randomly deposited colloidal particles. These findings motivated renewed interest in optically resonant nanoantennas that can be reproducibly fabricated (Haynes et al. 2003; Jackson et al. 2003; Rechberger et al. 2003; Su et al. 2003; Genov et al. 2004; Hao and Schatz 2004), which in turn led to our emphasis on metallic bowtie nanoantennas (see Figure 1.6) that are controllably produced using electron-beam lithography (EBL). Bowtie nanoantennas, designed to combine both the lightning-rod and coupled-plasmon resonant enhancement effects, should greatly improve the mismatch between conventional optical excitation and nanoscale objects, enabling progress in the area of nanophotonics.

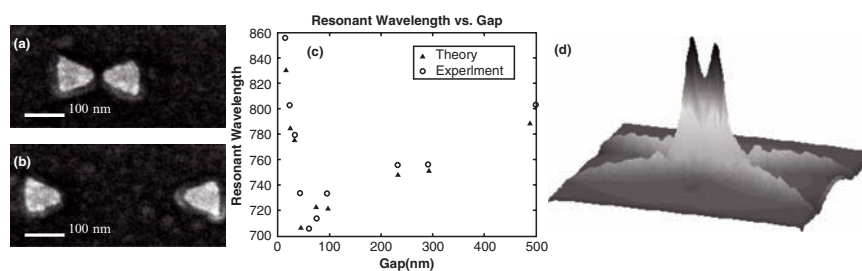


**Figure 1.6** SEM images of two representative gold bowties on a fused silica-ITO substrate (a) and (b). The variation of resonant wavelength with gap for light polarized along the line between the two triangles, with experiment shown as open circles and FDTD simulations as filled triangles (c). (After Sundaramurthy et al. (2005), used by permission.) FDTD simulation of field intensity ( $I$ ) enhancement near a 16 nm-gap bowtie (d) pumped at  $\lambda = 830$  nm. Maximum  $I$  enhancement is  $\sim 1500$ .

### 1.3.2 *Optically Resonant Metallic Bowtie Nanoantennas*

Initial studies were aimed at making reproducible sub-100 nm-sized metallic bowties that could be located at specified positions. To achieve this, Au bowties were fabricated with electron beam lithography (EBL) on transparent substrates. Details of bowtie nanoantenna fabrication can be found in Fromm et al. 2004 and scanning electron microscope (SEM) images of two representative bowties with different gap sizes are shown in Figure 1.6a,b. Each triangle of a bowtie is  $75 \pm 5$  nm in length (perpendicular bisector), has a tip radius of curvature of  $18 \pm 2$  nm, an Au thickness of  $\sim 18$  nm, and a 3.0 nm Ti adhesion sticking layer. Objects of this size are at the limit of current EBL fabrication methods.

Due to the complex behavior of metals at optical frequencies (Palik 1985), it is important to note that optically resonant nanoantennas are not “scaled-down” versions of their microwave and radiowave counterparts. The utilization of plasmon resonance effects is required to achieve antenna behavior in the optical regime, which results in antenna sizes that are much smaller than might be expected if “ideal” metallic properties are assumed.

### 1.3.3 *Optical Resonances of Metallic Bowtie Nanoantennas*

Because localized plasmon resonances are extremely dependent on geometry and material properties, we investigated the spectral scattering behavior of bowtie nanoantennas in detail, both experimentally (Fromm et al. 2004) and theoretically (Sundaramurthy et al. 2005) using finite-difference time-domain (FDTD) calculations of the local electromagnetic field. Single bowtie scattering spectra were measured experimentally as a function of gap size with far-field total internal reflection (TIR) microscopy. This method has the advantage that the excitation beam is trapped in the evanescent field until scattered toward the detector by the bowtie. The excitation light was broadband and s-polarized so that the axis of each bowtie was carefully oriented parallel to the polarization axis. (The perpendicular polarization leads to unremarkable results, similar to the scattering from isolated triangles (Fromm et al. 2004)).

Many bowties with varying gaps were fabricated and measured on a single substrate to record the peak scattering wavelength versus gap, with the results shown in Figure 1.6c. The measured results (open circles) were compared to three-dimensional FDTD calculations of the spectra, and the resonant wavelengths are shown as closed triangles. The FDTD simulations used measured frequency-dependent dielectric properties of the Au and simulated the exact structure fabricated, making no approximations to compute the final field intensity in the vicinity of the bowties.

Plotting the peak resonant wavelength as a function of gap size provides insight into the interparticle coupling behavior of single bowtie nanoantennas. Figure 1.6c shows the resonant scattering wavelength for 27 individual bowties, with gaps ranging from 16 to 488 nm, plotted against gap size. For light polarized along the line between the two triangles, the plasmon scattering resonance first blue-shifts with

increasing gap, and then red-shifts as the particles become more and more uncoupled; this was a surprising result as observations of the blue-shift followed by red-shift had not previously been reported in the literature.

This behavior may be approximately understood in a coupled-dipole approximation as changes in the phase between static dipole–dipole interactions and dipole radiative interaction effects (Zhao et al. 2003; Fromm et al. 2004). The peak resonance wavelengths from the FDTD simulations (closed triangles) agree quite well with the experimental observations, suggesting the utility of FDTD in predicting the behavior of coupled nanoparticle systems. Moreover, the calculations give information about the local electric fields and currents, which leads to the following interpretation of the resonant wavelength shifts. For gaps less than 60 nm, as shown in Figure 1.6a, the dominant field is between the tips. The gap capacity and the inductance due to plasmon propagation near the tip cause a resonance that shifts to the red as the gap size is decreased and the capacity increases. For gaps greater than 60 nm, the fields are predominantly in the  $y$ -direction normal to the triangles and flow back to the triangle from which they left. The device tends to behave more as a single triangle and has a resonance that shifts slowly to the red as the gap increases (Sundaramurthy et al. 2005).

### ***1.3.4 Local Enhancement of the Optical Fields Near the Nanoantenna***

Theoretical calculations suggest the plasmon resonances of such bowtie structures should be accompanied by extremely localized, greatly enhanced optical fields, which may be useful for a diverse range of future nanoscale applications. An FDTD-calculated field intensity distribution just above the bowtie surface is shown in Fig. 1.6d for a 16 nm-gap bowtie pumped near resonance with  $\lambda = 830$  nm radiation. According to the simulation, the fields are confined to regions approximately 20 nm in diameter ( $\sim\lambda/40$ ) near the tip of each triangle and should be enhanced by more than 1500 times relative to the intensity of the incident beam!

It had previously proven difficult to directly measure the electromagnetic fields in the gaps between plasmonically coupled structures because the incident pumping field extends over a much larger (diffraction-limited) area and tends to leak into the detector. To address this, we have found it useful to use two-photon effects that only appreciably occur in the regions where the optical fields are very strong. Using this approach, we have experimentally determined (Schuck et al. 2005a) the optical intensity enhancement values for the fields in the metal of these structures, which closely approximate the fields outside the metal near the surface.

Strongly enhanced local fields due to the excitation of surface plasmons in rough films, sharp tips, and nanoparticles give rise to detectable two-photon absorption in Au (Chen et al. 1981; Boyd et al. 1986; Beversluis et al. 2003). The resulting excitation of electrons from the  $d$  valence band to the  $sp$  conduction band leads to a broadband emission continuum, termed two-photon-excited photoluminescence (TPPL) in Au. Due to its nonlinear (intensity squared) dependence on excitation intensity, TPPL is an extremely sensitive probe of excitation field strength and

distribution. Variations between the TPPL spectra from differently shaped Au nanoparticles provide evidence for the localized origin of the absorption and subsequent emission (Bouhelier et al. 2003).

We have used TPPL to directly determine absolute values for optical field enhancements of single Au bowties by comparing the strength of TPPL from bowties with TPPL from a smooth Au film (Schuck et al. 2005a). The TPPL from individual bowties was measured with a sample-scanning microscope. A mode-locked Ti:sapphire laser producing high peak intensity 120 fs pulses at  $\lambda = 830$  nm with a repetition rate of 75 MHz was used for excitation. The value  $\lambda = 830$  nm was chosen because the smallest gap bowties were measured to be resonant close to this wavelength (see Figure 1.6c).

Using a diffraction-limited focus from an inverted microscope, arrays of single bowties with various gap sizes were scanned, and Au TPPL was focused onto a single-photon counting avalanche photodiode (APD) for broadband collection, creating TPPL images such as those shown in Figures 1.7a,b. Figures 1.7d,e show that the TPPL is strongly polarization-dependent. After optical experiments, the sample was coated with a thin Cr layer ( $\sim 4$  nm) to enable careful measurement of nanoantenna gap size in a scanning electron microscope (SEM).

The intensity enhancement factor in the metal of the bowtie  $i$ ,  $\alpha_{br}^i$ , can be calculated by carefully measuring the ratio of TPPL intensities from the bowtie and a smooth reference film and taking into the account the different excitation areas in the two cases (Schuck et al. 2005a). As shown in Figure 1.7c, the experimentally determined TPPL intensities yield  $E^2$  enhancement factors of greater than  $10^3$ , or greater than  $10^6$  in  $E^4$  (i.e.,  $\alpha^2$ ) for bowties with the smallest gaps. These are the largest such factors reported to date for lithographically produced nanoantennas. It should be noted that with gap spacings smaller than 16 nm and smaller tip radii of curvature than 12 nm, it should be possible in principle to obtain still stronger fields. However, smaller and well-controlled gap spacings and tip radii may be difficult to reliably fabricate in practice.

A comparison of Figure 1.7a with 1.7b demonstrates the practical limitations of EBL when attempting to produce ever-smaller gap sizes and features. Figure 1.7a is a TPPL image of four bowties, each designed to have 24 nm gaps. Note the general uniformity of the TPPL, evidence of consistent bowtie shape and gap size. There is a large variation in TPPL intensities, however, from the four bowties in the TPPL image in Figure 1.7b, which are from an array designed to contain bowties with significantly smaller (19 nm) gaps. In Figure 1.7b, the inhomogeneity in brightness results from variations in the actual gap width (gaps ranging from 0 to 28 nm were measured for this array), and bowties that appear dark were later found to be shorted using SEM.

### ***1.3.5 Exploring the Chemical Enhancement for Surface-Enhanced Raman Scattering with Au Bowtie Nanoantennas***

Over 30 years ago, it was first observed that the Raman signal of pyridine dramatically increases when adsorbed on a roughened Ag electrode (Fleischmann et al.

1974; Jeanmaire and Van Duyne 1977), and the detailed origins of surface-enhanced Raman scattering (SERS) arising from nanostructured metals have remained a topic of debate. Researchers have divided the SERS enhancements into two factors (Michaels, et al. 2000): an electromagnetic (EM) enhancement, where illumination intensity is enhanced due to sharp metal edges or plasmon effects, and a chemical enhancement (CE), where the Raman cross-section of adsorbed molecules is increased above the solution value (Moskovits 1985).

Interest in the SERS mechanism blossomed with the recent observation of Raman lines apparently arising from single molecules adsorbed onto colloidal Ag and Au particles (Kneipp et al. 1997; Nie and Emory 1997; Michaels et al. 2000). To obtain the 14-order of magnitude enhancement required to make Raman signals competitive with single-molecule fluorescence, it was believed that an enormous EM enhancement at “hot spots” was combined with a modest CE in these systems.

Michaels et al. (2000) suggested that coupled colloidal particles locally enhance the incident laser pump intensity and SERS detection probability, yielding a total EM enhancement potentially as high as  $10^{10}$ . However, uncertainty about the relative importance of the chemical effect, which has been estimated to enhance SERS signals by factors anywhere from 10 to as high as  $10^6$  (Otto 2002; Haran 2004), has motivated our use of bowties as an electromagnetically calibrated SERS-active substrate. Because bowties provide a coupled plasmon system with lithographically controllable gap and known (measured) EM enhancement (Schuck et al. 2005a), they allow direct exploration of the role of CE in SERS (Fromm et al. 2006).

For this study, bowties were coated with p-mercaptoaniline (pMA), which is known to form a self-assembled monolayer (SAM) upon binding to Au through the thiol. Using the known values for the monolayer packing area of pMA ( $19\text{\AA}^2/\text{molecule}$ ), the surface area of the bowtie experiencing enhanced E-fields ( $3000\text{nm}^2$ ) as predicted by electromagnetic calculations (Sundaramurthy et al. 2005), the solution-phase pMA Raman scattering cross-section for nonresonant, infrared pumping ( $10^{-29}\text{cm}^2$ ), and excitation and detection parameters, total SERS enhancement (TE) for pMA on the bowtie was estimated to be  $7 \times 10^7$  per molecule, assuming all  $10^4$  molecules in the enhanced field contribute equally to SERS. The TE value is often broken into EM and CE contributions in the following manner:  $\text{TE} = (|E|_{\text{pump}}^2 / |E_0|^2) \cdot (|E|_{\text{transmit}}^2 / |E_0|^2) \cdot \text{CE}$ , where  $E_0$  is the incident electric field. In our bowties,  $|E|_{\text{pump}}^2$  is measured (Schuck et al. 2005a) to be  $\sim 1500 \cdot |E_0|^2$ . Assuming that  $|E|_{\text{transmit}}^2$  is also  $\sim 1500 \cdot |E_0|^2$ , reasonable for Stokes radiation considering the fairly broad antenna resonance (Fromm et al. 2004), a value of CE  $\sim 30$  is obtained, consistent with previous estimates.

Closer examination of the SERS spectra reveals that there are intriguing and unexpected dynamics; particular lines “blink” and their mode frequencies shift discontinuously, even though an entire monolayer of pMA covers the bowtie. Behavior like this has been reported previously (Kneipp et al. 1997; Nie and Emory 1997; Michaels et al. 2000; Haran 2004), but only at concentrations of a few molecules per nanoparticle.

It is immediately obvious in the spectral waterfall plot in Figure 1.8A that the intensity and frequency of some Raman lines are stable, but vary significantly for other modes. Using previous pMA mode assignments (Osawa et al. 1994), modes

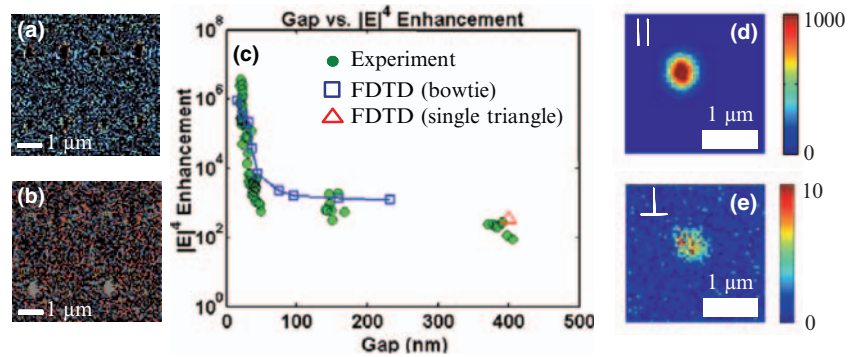


**Figure 1.7** TPPL images of bowties from arrays with nominal gap sizes of (a) 24 nm and (b) 19 nm. Comparison of experimental (circles) and theoretical (open squares and triangle) values of the square of intensity enhancement,  $(\alpha_{\text{pl}})^2$ , for bowties with gaps of 16 nm to 406 nm (c). FDTD simulations for  $(\alpha_{\text{pl}})^2$  from an individual triangle are used for comparison to the bowties with nominal gap size of 400 nm. Incident polarization dependence is shown in (c) and (d) for a 20 nm gap bowtie (note different scales). (After Schuck et al. (2005a), used by permission)

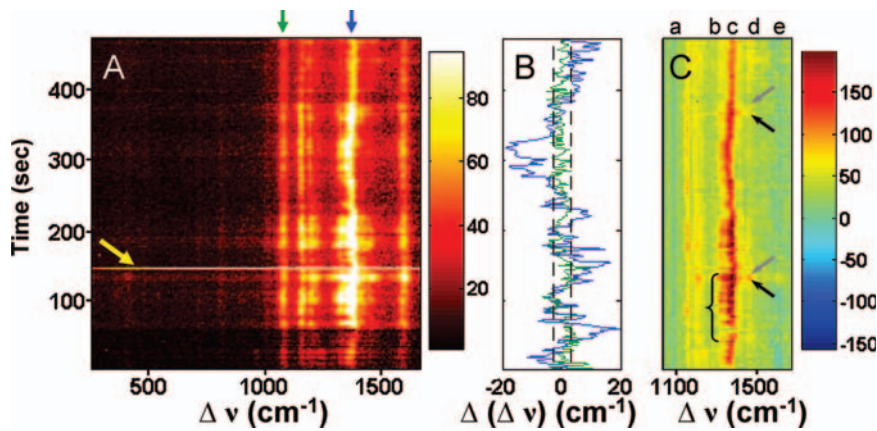


**Figure 1.8** (A) Waterfall plot showing the evolution of SERS spectra with time (2 s integration).  $I = 11 \text{ kW/cm}^2$  for  $t = 0 - 57 \text{ s}$ , and  $I = 38 \text{ kW/cm}^2$  for  $t = 57 - 460 \text{ s}$ . Notice the intense flash of continuum fluorescence at  $t \sim 150 \text{ s}$  (yellow arrow), the relatively stable modes at  $1077$  and  $1590 \text{ cm}^{-1}$ , and fluctuations of both frequency and amplitude for the  $1160$ ,  $1195$ ,  $1325$ ,  $1380$ , and  $1450 \text{ cm}^{-1}$  Raman modes. (B) Mode center frequency fluctuations for  $1077$  (green) and  $1380 \text{ cm}^{-1}$  (blue) lines, with error bar shown as dashed lines. Only modes with  $b_2$  symmetry fluctuate significantly. (C) A waterfall plot of difference spectra showing discrete intensity fluctuations evident for  $b_2$  modes. Note the blinking in the  $1325 \text{ cm}^{-1}$  mode (bracket, mode “b”) and “on” (black arrows) “off” (gray arrows) switching for mode “d,”  $1450 \text{ cm}^{-1}$ . Mode “c” ( $1380 \text{ cm}^{-1}$ ) also fluctuates. Modes (“a,”  $1077 \text{ cm}^{-1}$  and “e,”  $1590 \text{ cm}^{-1}$ ) having  $a_1$  symmetry are suppressed by the subtraction (see text and Fromm et al. (2006) for details). (After Fromm et al. (2006), used by permission)

at 1077 and 1590  $\text{cm}^{-1}$ , assigned to  $a_1$  symmetry, are stable in their frequency, and their intensity varies by less than a factor of 2 over the entire spectral series. For this reason, we use the  $a_1$  modes as key reference modes in our analysis below. Conversely, peaks at 1160, 1195, 1325, 1380, and 1450  $\text{cm}^{-1}$ , which have  $b_2$  symmetry and have been interpreted as charge transfer (CT) modes for pMA (Hill and Wehling 1993; Osawa et al. 1994), display large frequency and intensity fluctuations. For frequency fluctuations, Figure 1.8B displays the center frequency time trajectory of one mode in each of the two classes, determined by fitting the peaks to Lorentzian profiles. The  $a_1$  1077  $\text{cm}^{-1}$  reference mode (green) displays little change within the noise (dashed lines), whereas the  $b_2$  1380  $\text{cm}^{-1}$  mode (blue) varies significantly, often “jumping” as much as  $\pm 20 \text{ cm}^{-1}$  from its average value.

One may assume that the Raman spectra include contributions from a large number of molecules with the small enhancement calculated above, plus a contribution from a small number of molecules with large (possibly huge) enhancement. To highlight the latter contribution, we use the strength of the 1077  $\text{cm}^{-1}$  reference mode to scale a bulk pMA SERS calibration spectrum (measured elsewhere; Fromm et al. (2006)) and subtract it from the observed spectra, generating the difference spectra in Figure 1.8C. Note that scaling by the 1077  $\text{cm}^{-1}$  mode automatically makes the other  $a_1$  mode at 1590  $\text{cm}^{-1}$  disappear. Figure 1.8C shows strong on/off amplitude fluctuations in several  $b_2$  modes (designated “b” and “d”), for example, at the arrows and bracket. Because the  $b_2$  modes have been shown to be strongly affected by charge transfer (CT) from the metal (Osawa et al. 1994), the discrete fluctuations of the  $b_2$  modes suggest a dynamic CT process is occurring.

Due to the difficulty in synchronizing even a small number of molecules, discrete intensity fluctuations (blinking) and spectral jumping are often used as two spectroscopic signatures of single molecules (Moerner and Orrit 1999). We note that blinking alone is not necessarily a fair indicator of single-molecule SERS, because the EM enhancement could rapidly change, leading to temporary fluctuations of SERS signals for all molecules near the gap. The stability of the reference  $a_1$  modes shows that large EM changes are not occurring here.

Because the frequency and/or amplitude of the  $b_2$  modes often discontinuously “jump,” and in any one 2 s spectrum, a single frequency is observed, this observation implies that there is either a synchronization of a huge fraction of the  $10^4$  molecules near the gap (Fromm et al. 2006), or that a very small subset of molecules is responsible for the discontinuous changes, with the possibility that the fluctuating difference SERS signature is from just a few molecules. If this is true, the varying frequencies (Figure 1.8B) and amplitudes (Figure 1.8C) of the CT  $b_2$  modes suggest that selected molecule(s) are subject to a huge variation in their CE, from  $\sim 30$  to as much as  $\sim 10^7$ , whereupon CT temporarily increases the Raman cross-section of affected modes. Apparently, the signal from a small subset may be comparable, even exceeding (by more than an order of magnitude) that of the remaining  $10^4$  molecules near the bowtie gap, even though both are subject to the same EM value, not an unreasonable possibility (Wang 2005). This fascinating behavior may be possibly understood using existing CT theory, in which we suggest that an increase in wavefunction mixing between  $\pi$ -orbitals in the benzene ring and Au occurs when

a pMA molecule lies down at the surface. Tests of this idea would require careful imaging of the SAM in future studies.

## 1.4 Summary and Prospects

### 1.4.1 *Single-Molecule Fluorophores*

The DCDHF single-molecule fluorophores have been used in polymer hosts to report on local free volume through differences in the excited-state lifetime. The dyes have also been incorporated into the membranes of live cells for use as lipid analogues, and single copies can be observed diffusing in the cell membrane. Two-photon fluorescence has been observed for single DCDHF fluorophores as well. In future studies, the DCDHF fluorophores can be considered for situations where the molecule is specifically attached to a biomolecule or polymer or binds strongly to a biomolecule. When the molecule is located in a relatively rigid environment, the emission would be much brighter compared to the case where the molecule is unbound or is in a more flexible local environment. Another class of studies envisioned can take advantage of the large ground-state dipole moment; in particular, one would expect to be able to turn the molecule using an external electric field or a strong, time-varying local electric field such as that from the bowties. In addition, the optical nonlinearity of these molecules is a third local reporter variable that is waiting to be explored in imaging applications.

### 1.4.2 *Metallic Bowtie Nanoantennas*

In order to explore the regime where optical fields much smaller than the diffraction limit are used to probe molecules, we have fabricated Au bowtie nanoantennas by e-beam lithography that have tunable resonances in the visible/near-IR wavelength range. FDTD calculations have been used to predict resonance frequencies, field profiles, and local field enhancements. Experimental measurements of peak scattering wavelength by TIR microscopy for bowties with a range of gap sizes from 20 to 500 nm are in good agreement with theory. We have also experimentally measured optical intensity enhancements at Au bowtie nanoantennas of various gap sizes using TPPL, and the field intensity enhancement is  $>10^3$  confined to a region  $\sim 650 \text{ nm}^2$ . Because the electromagnetic enhancement is known for bowties, they have provided the first calibrated substrate for the direct investigation of the chemical enhancement effect in SERS, which may be as large as  $10^7$  for a few molecules.

It is to be expected that with optimization of the fabrication, Au bowties will be reproducibly manufactured either individually on a scanning probe or in large arrays on a single substrate. This would yield extremely intense near-field optical light sources with high local contrast that have applications ranging from ultra-sensitive

biological detection, single-molecule spectroscopy, and nanometer-scale lithography to high-resolution optical microscopy and spectroscopy.

Already, in recent work, the bowties have been used to fabricate ultra-small islands of photoresist by two-photon polymerization (Sundaramurthy et al. 2006). Using a bowtie to pump single molecules would be a dramatic improvement in the mismatch between conventional optical excitations and nanoscale structures. However, it will be essential to treat the molecule–bowtie system as a coupled near-field object in order to understand the observed effects, especially because there may be perturbation of the molecular properties by the proximity to the metal (Ambrose et al. 1994; Trautman et al. 1994; Bian et al. 1995). Eventually, these light sources will be combined with the ultimate small emitter, a nm-sized single molecule.

**Acknowledgments** This work was supported in part over the years by the U. S. Department of Energy Grant No. DE-FG03-00ER45815, by the National Institutes of Health Grant Nos. 1R21-GM65331 and 1P20-HG003638, and by the National Science Foundation Grant Nos. DMR-0237247 and DMR-0507296.

## References

- Albota, M.A., C. Xu, et al. (1998). Two-photon fluorescence excitation cross sections of biomolecular probes from 690 to 960 nm. *Appl. Opt.* **37**: 7352–7356.
- Ambrose, W.P., P.M. Goodwin, et al. (1994). Alterations of single molecule fluorescence lifetimes in near-field optical microscopy. *Science* **265**: 364–367.
- Barbara, P.F., A.J. Gesquiere, et al. (2005). Single-molecule spectroscopy of conjugated polymers. *Acc. Chem. Res.* **38**: 602–610.
- Barkai, E., Y.-J. Jung, et al. (2004). Theory of single-molecule spectroscopy: Beyond the ensemble average. *Annu. Rev. Phys. Chem.* **55**: 457–507.
- Betzig, E., J.K. Trautman, et al. (1991). Breaking the diffraction barrier: Optical microscopy on a nanometric scale. *Science* **251**: 1468–1470.
- Beyersluis, M.R., A. Bouhelier, et al. (2003). Continuum generation from single gold nanostructures through near-field mediated intraband transitions. *Phys. Rev. B* **68**: 115433.
- Bian, R.X., R.C. Dunn, et al. (1995). Single molecule emission characteristics in near field microscopy. *Phys. Rev. Lett.* **75**: 4772–4775.
- Bohn, J.L., D.J. Nesbitt, et al. (2001). Field enhancement in apertureless near-field scanning optical microscopy. *J. Opt. Soc. Amer. A* **18**(12): 2998–3006.
- Bouhelier, A., M.R. Beyersluis, et al. (2003). Characterization of nanoplasmonic structures by locally excited photoluminescence. *Appl. Phys. Lett.* **83**: 5041–5043.
- Boyd, G.T., Z.H. Yu, et al. (1986). Photoinduced luminescence from the noble metals and its enhancement on roughened surfaces. *Phys. Rev. B* **33**: 7923–7936.
- Burland, D.M., R.D. Miller, et al. (1994). Second-order nonlinearity of poled-polymer systems. *Chem. Rev.* **94**: 31–75.
- Chen, C.K., A.R.B. de Castro, et al. (1981). Surface enhanced second-harmonic generation. *Phys. Rev. Lett.* **46**: 145–148.
- Cotlet, M., S. Masuo, et al. (2004). Probing conformational dynamics in single donor–acceptor synthetic molecules by means of photoinduced reversible electron transfer. *Proc. Nat. Acad. Sci. USA* **101**: 13343–13348.
- Crozier, K.B., A. Sundaramurthy, et al. (2003). Optical antennas: Resonators for local field enhancement. *J. Appl. Phys.* **94**: 4632–4642.

- Denk, W., J.H. Strickler, et al. (1990). Two-photon laser scanning fluorescence microscopy. *Science* **248**: 73–76.
- Fleischmann, M., P.J. Hendra, et al. (1974). Raman spectra of pyridine adsorbed at a silver electrode. *Chem. Phys. Lett.* **26**(2): 163–166.
- Fromm, D.P., A. Sundaramurthy, et al. (2004). Gap-dependent optical coupling of single “bowtie” nanoantennas resonant in the visible. *Nano Lett.* **4**: 957–961.
- Fromm, D.P., A. Sundaramurthy, et al. (2006). Exploring the chemical enhancement for surface-enhanced Raman scattering with Au bowtie nanoantennas. *J. Chem. Phys. Commun.* **124**(6): 061101.
- Genov, D.A., A.K. Sarychev, et al. (2004). Resonant field enhancement from metal nanoparticle arrays. *Nano Lett.* **4**: 153–158.
- Grober, R.D., R.J. Schoelkopf, et al. (1997). Optical antenna: Towards a unity efficiency near-field optical probe. *Appl. Phys. Lett.* **70**: 1354–1356.
- Ha, T. (2001). Single-molecule fluorescence resonant energy transfer. *Methods* **25**: 78–86.
- Ha, T., T.A. Laurence, et al. (1999). Polarization spectroscopy of single fluorescent molecules. *J. Phys. Chem. B* **103**: 6839–6850.
- Hao, E. and G.C. Schatz (2004). Electromagnetic fields around silver nanoparticles and dimers. *J. Chem. Phys.* **120**: 357–366.
- Haran, G. (2004). Single molecule-Raman spectroscopy and local work function fluctuations. *Israel J. Chem.* **44**: 385–390.
- Hartschuh, A., E.J. Sanchez, et al. (2003). High-resolution near-field Raman microscopy of single-walled carbon nanotubes. *Phys. Rev. Lett.* **90**: 95503.
- Haynes, C.L., A.D. McFarland, et al. (2003). Nanoparticle optics: The importance of radiative dipole coupling in two-dimensional nanoparticle arrays. *J. Phys. Chem. B* **107**: 7337–7342.
- He, M., R. Twieg, et al. (2002). Dicyanomethylenedihydrofuran photorefractive materials. *Proc. SPIE* **4802**: 9–20.
- Hill, W. and B. Wehling (1993). Potential- and pH-dependent surface-enhanced Raman scattering of p-mercapto aniline on silver and gold substrates. *J. Phys. Chem.* **97**: 9451–9455.
- Hummer, G. and A. Szabo (2005). Free energy surfaces from single-molecule force spectroscopy. *Acc. Chem. Res.* **38**: 504–513.
- Jackson, J.B., S.L. Westcott, et al. (2003). Controlling the surface enhanced Raman effect via the nanoshell geometry. *Appl. Phys. Lett.* **82**: 257–259.
- Jeanmaire, D.L. and R.P. Van Duyne (1977). Surface Raman spectroelectrochemistry Part I. Heterocyclic, aromatic, and aliphatic amines adsorbed on the anodized silver electrode. *J. Electroanal. Chem.* **84**(1): 1–20.
- Jin, L., A.C. Millard, et al. (2005). Cholesterol-enriched lipid domains can be visualized by di-4-ANEPPDHQ with linear and nonlinear optics. *Biophys. J.* **89**(1): L04–6.
- Kanis, D.R., M.A. Ratner, et al. (1994). Design and construction of molecular assemblies with large second-order optical nonlinearities. Quantum chemical aspects. *Chem. Rev.* **94**: 195–242.
- Kippelen, B., F. Meyers, et al. (1997). Chromophore design for photorefractive applications. *J. Amer. Chem. Soc.* **119**(19): 4559–4560.
- Kneipp, K., H. Kneipp, et al. (2002). Surface-enhanced Raman scattering and biophysics. *J. Phys. Condens. Mat.* **14**: R597–R624.
- Kneipp, K., Y. Wang, et al. (1997). Single molecule detection using surface-enhanced Raman scattering. *Phys. Rev. Lett.* **78**: 1667–1105.
- Kuzyk, M.G. and C.W. Dirk (1998). *Characterization Techniques and Tabulations for Organic Nonlinear Optical Materials*. New York: Dekker-CRC Press.
- Lakowicz, J.R. (1999). *Principles of Fluorescence Spectroscopy*. New York: Kluwer Academic.
- Lee, T.-H., J.I. Gonzales, et al. (2005). Single-molecule optoelectronics. *Acc. Chem. Res.* **38**: 534–541.
- Lord, S.J., Z. Lu, et al. (2007). Photophysical properties of acene DCDHF fluorophores: Long-wavelength single-molecule emitters designed for cellular imaging. *J. Phys. Chem. A* published on Web 8/24/2007, “<http://dx.doi.org/10.1021/jp0712598>” 10.1021/jp0712598.

- Lounis, B.L. and M. Orrit (2005). Single-photon sources. *Rep. Prog. Phys.* **68**: 1129–1179.
- Lu, H.P. (2005). Probing single-molecule protein dynamics. *Acc. Chem. Res.* **38**: 557–565.
- Maier, O., V. Oberle, et al. (2002). Fluorescent lipid probes: Some properties and applications. *Chem. Phys. Lipids* **116**: 3–18.
- Melikian, G., F.P. Rouessac, et al. (1995). Synthesis of substituted dicyanomethylendihydrofurans. *Synth. Commun.* **25**(19): 3045–3051.
- Michaels, A.M., J. Jiang, et al. (2000). Ag nanocrystal junctions as the site for surface-enhanced Raman scattering of single rhodamine 6G molecules. *J. Phys. Chem. B* **104**: 11965–11971.
- Moerner, W.E. (1997). Those blinking single molecules. *Science* **277**: 1059.
- Moerner, W.E. (2003). Optical measurements of single molecules in cells. *Trends Analyt. Chem.* **22**: 544–548.
- Moerner, W.E. (2004). Single-photon sources based on single molecules in solids. *New J. Phys.* **6**: 88.
- Moerner, W.E. and D.P. Fromm (2003). Methods of single-molecule fluorescence spectroscopy and microscopy. *Rev. Sci. Instrum.* **74**: 3597–3619.
- Moerner, W.E. and M. Orrit (1999). Illuminating single molecules in condensed matter. *Science* **283**: 1670–1676.
- Moskovits, M. (1985). Surface-enhanced spectroscopy. *Rev. Mod. Phys.* **57**: 783–826.
- Nalwa, H.S. and S. Miyata (Eds.) (1997). *Nonlinear Optics of Organic Molecules and Polymers*. Boca Raton, FL: CRC Press.
- Nicoud, J.F. and R.J. Twieg (1987). *Design and Synthesis of Organic Molecular Compounds for Efficient Second Harmonic Generation. Nonlinear Optical Properties of Organic Molecules and Crystals*. D. S. Chemla and J. Zyss. New York: Academic Press. **1**: 227–296.
- Nie, S. and S.R. Emory (1997). Probing single molecules and single nanoparticles by surface-enhanced Raman scattering. *Science* **275**: 1102–1106.
- Nishimura, S.Y., S.J. Lord, L.O. Klein, K.A. Willets, M. He, Z. Lu, R.J. Twieg, and W.E. Moerner (2006). Diffusion of lipid-like single-molecule fluorophores in the cell membrane. *J. Phys. Chem. B* **110**: 8151–8157.
- Novotny, L., E.J. Sanchez, et al. (1998). Near-field optical imaging using metal tips illuminated by higher-order Hermite–Gaussian beams. *Ultramicroscopy* **71**: 21–29.
- Osawa, M., N. Matsuda, et al. (1994). Charge transfer resonance Raman process in surface-enhanced Raman scattering from p-aminothiophenol adsorbed on silver: Herzberg-Teller contribution. *J. Phys. Chem.* **98**: 12702–12707.
- Ostroverkhova, O. and W.E. Moerner (2004). Organic photorefractives: Mechanisms, materials, and applications. *Chem. Revs.* **104**: 3267–3314.
- Ostroverkhova, O., D. Wright, et al. (2002). Recent advances in the understanding and development of photorefractive polymers and glasses. *Adv. Funct. Mater.* **12**(9): 621–629.
- Otto, A. (2002). What is observed in single molecule SERS, and why? *J. Raman Spectrosc.* **33**(8): 593–598.
- Palik, E.D. (1985). *Handbook of Optical Constants*. Orlando, FL: Academic Press.
- Parasassi, T., E.K. Krasnowska, et al. (1998). Laurdan and prodan as polarity-sensitive fluorescent membrane probes. *J. Fluoresc.* **8**: 365–373.
- Prasad, P.N. and D.J. Williams (1991). *Introduction to Nonlinear Optical Effects in Molecules and Polymers*. New York: John Wiley.
- Rasnik, I., S.A. McKinney, et al. (2005). Surfaces and orientations: Much to FRET about? *Acc. Chem. Res.* **38**: 542–548.
- Rechberger, W., A. Hohenau, et al. (2003). Optical properties of two interacting gold nanoparticles. *Opt. Commun.* **220**: 137–141.
- Schuck, P.J., D.P. Fromm, et al. (2005a). Improving the mismatch between light and nanoscale objects with gold bowtie nanoantennas. *Phys. Rev. Lett.* **94**: 017402.
- Schuck, P.J., K.A. Willets, et al. (2005b). A novel fluorophore for two-photon-excited single-molecule fluorescence. *Chem. Phys.* **318**: 7–11.
- Schütz, G.J., G. Kada, et al. (2000). Properties of lipid microdomains in a muscle cell membrane visualized by single molecule microscopy. *EMBO J.* **19**: 892–901.

- Soper, S.A., H.L. Nutter, et al. (1993). The photophysical constants of several fluorescent dyes pertaining to ultrasensitive fluorescence spectroscopy. *Photochem. Photobiol.* **57**: 972–977.
- Su, K.H., Q.-H. Wei, et al. (2003). Interparticle coupling effects on plasmon resonances of nanogold particles. *Nano Lett.* **3**: 1087–1090.
- Sundaramurthy, A., K.B. Crozier, et al. (2005). Field enhancement and gap-dependent resonance in a system of two opposing tip-to-tip Au nanotriangles. *Phys. Rev. B* **72**: 165409.
- Sundaramurthy, A., P.J. Schuck, et al. (2006). Toward nanometer-scale optical photolithography: Using the near-field of bowtie optical nanoantennas. *Nano Lett.* **6**: 355–360.
- Toutchkine, A., V. Kraynov, et al. (2003). Solvent-sensitive dyes to report protein conformational changes in living cells. *J. Amer. Chem. Soc.* **125**: 4132–4145.
- Trautman, J.K., J.J. Macklin, et al. (1994). Near-field spectroscopy of single molecules at room temperature. *Nature* **369**: 40–42.
- Tsien, R.Y. and A. Waggoner (1995). Fluorophores for confocal microscopy. *Handbook of Biological Confocal Microscopy 2nd ed.* J.B. Pawley. New York: Plenum Press, 267–279.
- Vallee, R.A.L., M. Cotlet, et al. (2004). Single-molecule conformations probe free volume in polymers. *J. Amer. Chem. Soc.* **126**: 2296–2297.
- Vrljic, M., S.Y. Nishimura, et al. (2002). Translational diffusion of individual class II MHC membrane proteins in cells. *Biophys. J.* **83**: 2681–2692.
- Wang, Z., Rothberg, L.J. (2005). Origins of blinking in single-molecule raman spectroscopy. *J Chem Phys B*: jp0460947.
- Watkins, L.P. and H. Yang (2004). Information bounds and optimal analysis of dynamic single-molecule measurements. *Biophys. J.* **86**: 4015–4029.
- Weiss, S. (1999). Fluorescence spectroscopy of single biomolecules. *Science* **283**: 1676–1683.
- Willetts, K.A., P.R. Callis, et al. (2004). Experimental and theoretical investigations of environmentally sensitive single-molecule fluorophores. *J. Phys. Chem. B* **108**: 10465–10473.
- Willetts, K.A., S.Y. Nishimura, et al. (2005). Nonlinear optical chromophores as nanoscale emitters for single-molecule spectroscopy. *Acc. Chem. Res.* **38**(7): 549–556.
- Willetts, K.A., O. Ostroverkhova, et al. (2003a). New fluorophores for single-molecule spectroscopy. *J. Amer. Chem. Soc.* **125**: 1174–1175.
- Willetts, K.A., O. Ostroverkhova, et al. (2003b). Novel fluorophores for single-molecule imaging. *Proc. SPIE* **5222**: 150–157.
- Wright, D., U. Gubler, et al. (2001). A high performance photorefractive polymer composite with 2-dicyanomethylene-3-cyano-2,5-dihydrofuran chromophore. *Appl. Phys. Lett.* **79**(26): 4274–4276.
- Xu, C. and W.W. Webb (1996a). Measurement of two-photon excitation cross sections of molecular fluorophores with data from 690 to 1050 nm. *J. Opt. Soc. Amer. B* **13**: 481–491.
- Xu, C., W. Zipfel, et al. (1996b). Multiphoton fluorescence excitation: New spectral windows for biological nonlinear spectroscopy. *Proc. Nat. Acad. Sci. USA* **93**: 10763–10768.
- Xu, H. and M. Kaell (2003). Polarization-dependent surface-enhanced Raman spectroscopy of isolated silver nanoaggregates. *Chem. Phys. Chem.* **4**: 1001–1005.
- Zenhausen, F., Y. Martin, et al. (1995). Scanning interferometric apertureless microscopy: Optical imaging at 10 angstrom resolution. *Science* **269**: 1083–1085.
- Zhang, C., C.G. Wang, et al. (2001). Progress toward device-quality second-order nonlinear optical materials. 4. A trilink high mu beta NLO chromophore in thermoset polyurethane: A “guest-host” approach to larger electrooptic coefficients. *Macromol.* **34**: 253–261.
- Zhao, L., K.L. Kelly, et al. (2003). The extinction spectra of silver nanoparticle arrays: Influence of array structure on plasmon resonance wavelength and width. *J. Phys. Chem. B*, **107**: 7343–7350.
- Zhuang, X. and M. Rief (2000). Single-molecule protein folding. *Curr. Opin. Struct. Biol.* **13**: 88–97.
- Zyss, J., Ed. (1994). *Molecular Nonlinear Optics*. New York: Academic Press.